

1

Viscoelastic Worm-Like Micelles in Nonionic Fluorinated Surfactant Systems

Suraj Chandra Sharma, Masahiko Abe, and Kenji Aramaki

1.1 Introduction

Perfluorosurfactants, like their hydrocarbon counterparts, form spherical micelles, rod-like micelles, vesicles, lamellar aggregates, and other various liquid-crystalline structures in solution, and the aggregate structures in fluorinated surfactants can be explained, like hydrocarbon surfactants, in terms of the value of critical packing parameter [1], $CPP = \nu/a_s l$, where ν is the volume of the hydrophobic part, l its length, and a_s the average area of headgroup at the interface. Similar phase sequence is observed in fluorinated surfactant and hydrocarbon surfactant systems when surfactant concentration is changed. However, perfluorosurfactants also exhibit major important differences from hydrocarbon surfactants. They are more hydrophobic and reduce the surface tension of water to an extent, which is in general unattainable with hydrocarbon surfactants. Similarly, they show a much lower critical micelle concentration than the hydrocarbon chain surfactants of the same length do [2, 3]. Perfluorosurfactants have stiff hydrophobic chains, with their skeleton covered by a dense electron-rich environment. It is easier to pack fluorocarbon chains closely because the chains are in the all-*trans* state and less entropy is lost. As a result, these surfactants have high chemical and thermal stability. The good chemical and thermal stability of fluorocarbon surfactants is an important consideration to operate in harsh environment such as extremes of pH, high temperatures or in combination with strong oxidizing or reducing agents. Since the fluorocarbon chains are bulkier than the hydrocarbon chain, with the volume of $-\text{CF}_2$ and terminal $-\text{CF}_3$ being higher than that of the $-\text{CH}_2$ and $-\text{CH}_3$, respectively [4], a fluorinated surfactant having a very large headgroup is needed to form a spherical aggregate ($CPP \leq 1/3$), to balance the effect of bulky fluorocarbon chain [5]. Therefore, cylindrical micelles are often observed in fluorinated surfactant systems at solution conditions where spherical micelles are expected in hydrocarbon surfactant systems. These cylindrical micelles often undergo enormous one-dimensional growth and form very long and flexible aggregates, referred to as “worm-like” micelles, for which the spontaneous curvature of the end-caps is higher than the curvature along the cylindrical body. The growth

is therefore a consequence of the system to minimize the excess free energy by reducing the number of end-caps in spite of the counteracting entropy factor. When the number density of the worm-like aggregates exceeds a certain threshold value, they entangle with each other to form a transient network, similar to a solution of flexible polymers and display remarkable viscoelastic properties.

The formation and properties of viscoelastic worm-like micelles have been studied extensively, mostly in long hydrophobic chain cationic surfactant [6–15] in the presence of high concentrations of salt, which screens the electrostatic repulsions between the charged surfactant headgroups. Viscoelastic solutions of worm-like micelles have also been reported in cationic or anionic fluorinated surfactant aqueous systems, even at a relatively short fluorocarbon chain length [16–18]. The effect of the concentration of counterions and surfactant concentration on the rheological behavior and micellar growth is more or less similar in both types of surfactants [18]. There are studies on the thermoresponsive viscoelasticity in some hybrid anionic surfactants containing both fluorocarbon and hydrocarbon chain in their molecules [19–22]. Although the majority of worm-like micelles systems reported are charged, nonionic surfactants, such as ethoxylated sterols [23–25] and sucrose alkanolates [26] can also form worm-like micelles. In these systems, interfacial curvature of the aggregates can be tuned to induce sphere–rod transition and one-dimensional micellar growth via the addition of a lipophilic surfactant, such as polyoxyethylene alkyl ether or long-chain monoglyceride. A similar tendency is observed in ionic surfactants solution as well [27–31]. An aqueous solution of a surfactant with a cholesteric group as the hydrophobic part formed a viscoelastic solution at elevated temperature [32]. Knowledge about the formation and rheological properties of nonionic systems is important not only to obtain a better understanding of the underlying basic principle of the phenomenon, but also for practical applications such as in cosmetics and toiletry products because of the absence of charged species and improved mildness to the skin.

In this chapter, a brief theoretical background on the rheological behavior of viscoelastic worm-like micelles is given. It is followed by a discussion on the temperature-induced viscosity growth in a water–surfactant binary system of a nonionic fluorinated surfactant at various concentrations. Finally, some recent results on the formation of viscoelastic worm-like micelles in mixed nonionic fluorinated surfactants in an aqueous system are presented.

1.2

Rheological Behavior of Worm-Like Micelles

The viscoelasticity of the worm-like micelles arises because of the entanglement of very long and flexible worm-like micelles to form a transient network, similar to a solution of flexible polymers. Unlike polymers, however, worm-like micelles break and re-form dynamically. When the network of worm-like micelles is deformed or the equilibrium conditions are suddenly changed, the relaxation occurs within a definite time, and the equilibrium condition is restored again. For a deformation with a time period shorter than the relaxation time, τ_R , the system

exhibits an elastic property characteristic of a solid material with a Hookean constant, G_o , called the shear modulus. For a slow deformation, however, the network has sufficient time to dissipate the stress, and the viscoelastic system behaves as a viscous fluid with a zero-shear viscosity, η_o .

The rheological behavior of a viscoelastic material can be investigated by applying a small-amplitude sinusoidal deformation. The behavior can be described by a mechanical model, called the Maxwell model [33], consisting of an elastic spring with the Hookean constant, G_o , and a dashpot with the viscosity, η_o . The variation of storage modulus (G') and loss modulus (G'') with shear frequency, ω , are given by the equations

$$G'(\omega) = \frac{\omega^2 \tau_R^2}{1 + \omega^2 \tau_R^2} G_o \quad (1.1)$$

$$G''(\omega) = \frac{\omega \tau_R}{1 + \omega^2 \tau_R^2} G_o \quad (1.2)$$

where τ_R is the relaxation time. The parameters G' and G'' are the elastic and viscous components of the complex shear modulus, and they are related to the ability of the material to behave as an elastic or viscous material. As is evident from the Maxwell equations, in the low-frequency region, $\omega \ll \omega_c$, G' and G'' scale with ω according to $G' \approx \omega^2$ and $G'' \approx \omega$. In the high-frequency region, or more specifically, in the region of $\omega \gg \omega_c$, however, G' attains a plateau value equal to G_o , whereas G'' shows a monotonic decrease. The shear frequency corresponding to the $G'-G''$ crossover, ω_c , is equal to the inverse of τ_R . For worm-like micelles at particular conditions, the magnitude of τ_R is related to the average length of the worm-like micelles, whereas G_o is related to the number density of entanglement in the transient network.

Once G_o and τ_R are known, η_o can be calculated using the following relation:

$$\eta_o = G_o \tau_R \quad (1.3)$$

Alternately, the following relationship allows one to estimate η_o by extrapolating the complex viscosity values ($|\eta^*|$) to zero shear frequency:

$$|\eta^*| = \frac{(G'^2 + G''^2)^{1/2}}{\omega} = \frac{\eta_o}{\sqrt{1 + \omega^2 \tau_R^2}} \quad (1.4)$$

The living-polymer model proposed by Cates and coworkers [34–36] considers the molecular-weight distribution (MWD) of the worm-like micelle to be in a thermal equilibrium, and such systems are called an equilibrium polymer or “living polymer”, which is in contrast to the fixed MWD of ordinary polymer solutions. The viscoelastic behavior of the entangled worm-like micelles is described by considering two processes, reptation (i.e. reptile-like motion of the micelle along its own contour) and reversible scission of micelles, taking place at two time scales, namely, reptation time, τ_{rep} , and breaking time, τ_b . The τ_{rep} is the time required for a worm-like micelle of contour length \bar{L} to pass through a hypothetical tube, and the τ_b is the average time necessary for a chain of average length \bar{L} to break into two pieces. It is assumed that when a chain breaks, the two daughter chains

become uncorrelated and recombine with the micellar end in random way. For fast scission kinetics ($\tau_b \ll \tau_{\text{rep}}$), a single-exponential stress decay is observed, and the viscoelastic behavior of such systems at low-frequency follows Maxwell model with a single relaxation time, τ_R given by $(\tau_b \tau_{\text{rep}})^{1/2}$ [34].

Although the Maxwell equations predict a monotonous decrease of G'' in the high-frequency region, the worm-like micelles deviate from this behavior, showing an increase of G'' in the high-frequency region and a deviation from the semicircle, as well as a depression in a Cole–Cole plot of G' versus G'' . This deviation is often associated with the stress relaxation by additional ‘faster’ processes such as Rouse modes of cylindrical micelles, analogous to polymer chain. The value of G'' at the minimum, G''_{min} , can be related to contour length, \bar{L} according to the relation [35]

$$\frac{G''_{\text{min}}}{G_o} \approx \frac{l_e}{\bar{L}} \quad (1.5)$$

where l_e is the entanglement length, the contour length of the section of worm-like micelles between two entanglement points. For flexible micelles, the correlation length, ξ , which gives the mesh size of the micellar network, is related to l_e according to the relations [35]

$$l_e \approx \xi^{5/3} / l_p^{2/3} \quad (1.6)$$

The persistence length, l_p , gives an estimate of micellar flexibility. Even though the micelles are flexible, at a small length scale comparable to l_p , they behave as rigid rods. Also,

$$\xi = \left(\frac{kT}{G_o} \right)^{1/3} \quad (1.7)$$

Combining Eqs. (1.6) and (1.7) yields a relation which relates l_e to G_o [35]

$$G_o \approx \frac{kT}{l_e^{9/5} / l_p^{6/5}} \quad (1.8)$$

In the limit $\tau_b \ll \tau_{\text{rep}}$, the theoretical model predicts the following scaling laws for the viscoelastic parameters as a function of the volume fraction of surfactant (ϕ): [36]

$$G_o \approx \phi^{2.25} \quad (1.9)$$

$$\tau_R \approx \phi^{1.25} \quad (1.10)$$

$$\eta_o \approx \phi^{3.5} \quad (1.11)$$

1.3

Viscoelastic Worm-Like Micelles in Nonionic Fluorinated Surfactant System (Without Additives)

Recently, an aqueous solution of perfluoroalkyl sulfonamide ethoxylate, $C_8F_{17}SO_2N(C_3H_7)(C_2H_4O)_{10}H$, designated as $C_8F_{17}EO_{10}$ having a medium chain length (C_8)

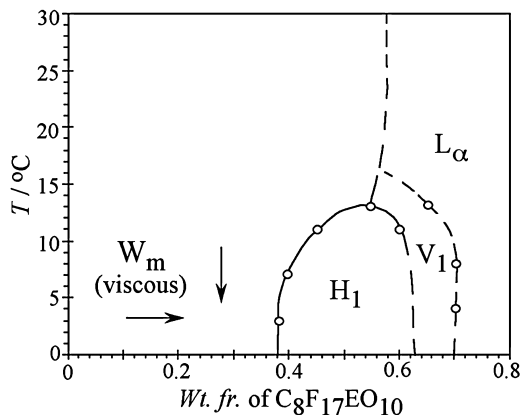


Figure 1.1 Partial phase diagram of $C_8F_{17}EO_{10}$ /water binary system. W_m stands for the micellar solution, and H_1 , V_1 , and L_α stand for hexagonal, bicontinuous cubic, and lamellar liquid crystalline phases. The arrows in the W_m domain show the direction of

viscosity increase for the systems at surfactant concentration of 15 wt% and above. At lower concentrations, viscosity increases and then decreases with increasing temperature (redrawn from Ref. [37]).

fluoroalkyl chain and relatively large headgroup (EO_{10}) has been reported to form highly viscoelastic solution of worm-like micelles at low temperatures [37]. The partial binary phase diagram of $C_8F_{17}EO_{10}$ /water system is shown in Figure 1.1. This is a typical phase diagram of a nonionic surfactant, such as polyoxyethylene alkylethers (C_mEO_n) [38], with a close resemblance to the phase diagram of $C_{12}EO_6$. With increasing surfactant concentration, an aqueous micellar solution (W_m), hexagonal (H_1), bicontinuous cubic (V_1), and lamellar (L_α) liquid crystalline phases are formed successively at low temperature. Micellar solutions at low temperature become increasingly viscous with increasing surfactant concentration, and at compositions near the H_1 phase, a highly viscous or gel-like solution is formed. This gel-like solution is isotropic and does not show any sharp diffraction peak in the small-angle X-ray scattering (SAXS) spectra, which rules out possibility of the presence of the discontinuous cubic (I_1) phase. Moreover, the fact that the viscosity of the solution gradually increases with increasing concentration also indicates that the I_1 phase is not present. In fact, the formation of globular micelles is not favorable because of bulky and stiff fluorinated chain unless the headgroup is very big. With increasing temperature, the viscosity of the solution gradually decreases and finally a less viscous easily flowing isotropic solution is formed. At higher temperature, a phase separation occurs at the cloud point, which is typical of nonionic surfactant systems. Esquena *et al.* [39] have constructed the aqueous binary phase behavior of the present system over wide ranges of temperature and composition.

Figure 1.2 shows the variation of viscosity (η) as a function of shear-rate ($\dot{\gamma}$) for 1 wt% surfactant solution at different temperatures. At low temperature (5°C), η

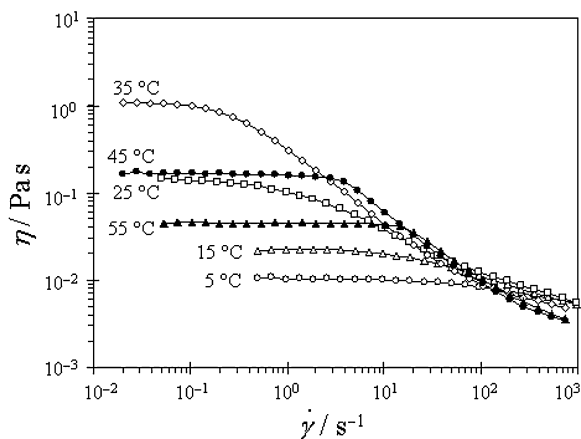


Figure 1.2 Steady shear-rate ($\dot{\gamma}$) vs. viscosity (η) curves of 1 wt% surfactant system at various temperatures (from Ref. [37]).

is independent of $\dot{\gamma}$, that is, Newtonian flow behavior is observed up to $\dot{\gamma} \sim 100 \text{ s}^{-1}$. At higher values of $\dot{\gamma}$ ($>100 \text{ s}^{-1}$), the viscosity decreases with increasing $\dot{\gamma}$, and this “shear thinning” behavior is typical of worm-like micelles. It should be that the viscosity of the surfactant solution is significantly higher than that of water or micellar solutions generally observed in surfactants solutions at such a low concentration of 1 wt%. Therefore, cylindrical micelles are expected to be present even at low temperatures. Upon an increase of temperature up to 35 °C, the critical $\dot{\gamma}$ for shear thinning shifts gradually to lower value and also the viscosity in the plateau region (low $\dot{\gamma}$) increases. This suggests that the system is becoming more “structured” with increasing temperature. When the temperature is increased further to 45 °C, the viscosity decreases and the Newtonian region appears up to higher $\dot{\gamma}$, which corresponds to the structural modification in the system. A comparison of the steady shear-rate curves at 25 and 45 °C shows that, although the viscosity at plateau region (low $\dot{\gamma}$) is nearly the same, the shear thinning behavior at higher shear-rate is not similar, which might be the result of a difference in the structure of the system at the respective temperatures. Rheological measurements were carried out only up to 55 °C because phase separation occurs at higher temperature.

The increase of viscosity with temperature in the nonionic surfactant can be understood in terms of the decrease in the interfacial curvature of the aggregates due to progressive dehydration of the EO chain. This would induce a sphere–rod transition in the aggregate shape or induce one-dimensional growth if the rod-like aggregates are already formed. Formation of end-caps in the cylindrical aggregates becomes unfavorable with increasing temperature because of the high free-energy cost of the formation of hemispherical ends and consequently one-dimensional growth is favored. The trend observed up to 35 °C is consistent with that view. However, above 35 °C, a turning point occurs and viscosity begins to decrease as

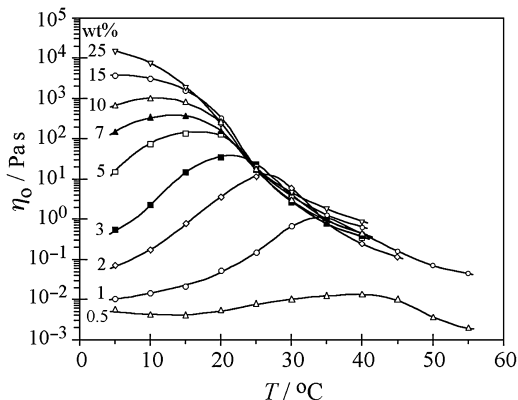


Figure 1.3 Variation of zero-shear viscosity (η_0) as a function of temperature at different concentrations (in wt%) of surfactant in water (from Ref. [37]).

if the micellar length changes in the opposite direction, possibly due to an increase in the extent of micellar scission kinetics. The explanation for this change in the rheological behavior is that with increasing temperature, the energy cost of the free ends of the micelles become higher, and therefore the free ends would fuse at the cylindrical part of its own or other micelles, thus forming micellar joints, or branching in the network structure. Such joints can slip along the cylindrical body, thereby allowing a faster and easier way of stress relaxation [40, 41]. Branching points also restricts the alignment of micelles under shear [42], causing an increase in critical $\dot{\gamma}$. In a number of surfactant systems, such micellar connections or branching points have been detected by cryogenic transmission electron microscopy [43–46].

Figure 1.3 shows the variation of zero-shear viscosity (η_0) as a function of temperature at different surfactant compositions. At 0.5 wt% surfactant concentration, the viscosity of the solution is low, and a gradual but small increase in viscosity is observed with increasing temperature up to 40 °C; then it decreases with a further increase in temperature and ultimately a phase separation takes place. For 1 wt% surfactant concentration, the increase in viscosity with an increase in temperature is clearly visible, with an increase of about 2 orders of magnitude in viscosity upon increasing temperature from 5 to 35 °C, and finally, the viscosity decreases with a further increase in temperature. The trend of the viscosity–temperature curve is essentially similar with increasing surfactant concentration, but the temperature for the viscosity maximum ($T_{\eta\text{-max}}$) gradually shifts to a lower value, and there is a significant increase in the viscosity at temperatures below $T_{\eta\text{-max}}$. Highly viscoelastic solutions are formed at low temperatures and high surfactant concentration. For 25 wt% surfactant concentration, the viscosity decreases with increasing temperature from 5 °C, and judging from the trends of curves, $T_{\eta\text{-max}}$ is well below 5 °C, but the behavior is essentially the same as that observed at lower concentrations. The viscosity of the micellar solution is very sensitive to the concentration at low

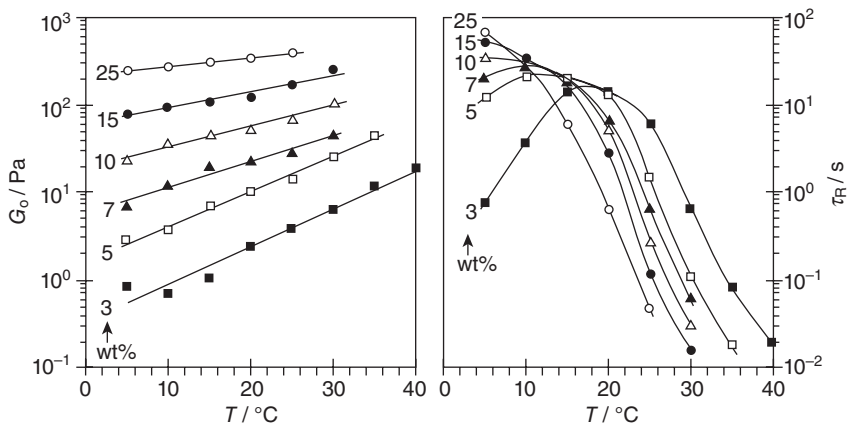


Figure 1.4 Variation of shear modulus (G_0) and stress relaxation time (τ_R) as a function of temperature at different concentrations (in wt%) of surfactant in water (from Ref. [37]).

temperatures, but at and above 25 °C, the viscosity is nearly the same over a wide range of concentrations (2–25 wt%).

With increasing surfactant concentration, the degree of hydration of the ethylene oxide chain decreases. The decrease in the hydration would decrease the spontaneous curvature of the aggregate and hence the energy required for the formation of hemispherical end-caps of the cylindrical micelles increases. Consequently, one-dimensional micellar growth is favored and viscosity increases. Therefore, the effect of increasing surfactant concentration is similar to that of increasing temperature. Formation of micellar joints is expected to take place at lower temperatures with increasing surfactant concentration and, hence the viscosity maximum shifts gradually toward the lower temperature.

The estimated values for G_0 and τ_R are plotted as a function of temperature at different surfactant concentrations as shown in Figure 1.4. It can be seen that G_0 increases monotonically with increasing temperature, which may be taken as evidence of an increase in the network density of the worm-like micelles at all concentrations. However, the extent of the increase of G_0 with temperature decreases with increasing surfactant concentration. At 3 wt% surfactant concentration, G_0 increases by 1 order of magnitude when temperature changes by 20 °C, whereas at 25 wt% the change is significantly small.

On the other hand, the τ_R of the viscoelastic solutions at low concentrations, for example, in a 3 wt% surfactant system, first increases promptly with increasing temperature, reaches the maximum value at ~20 °C, and then decreases. When the surfactant concentration increases from 3 to 5 wt% and above, the trend remains essentially the same, but the position of the τ_R maximum slowly moves to lower temperature. At higher concentrations of surfactant (e.g., at 10 and 15 wt%), the τ_R maxima are around 5 °C. No maximum is seen at 25 wt% surfactant concentration, but τ_R starts decreasing from 5 °C. However, judging from the trends of the τ_R – T curves, the τ_R maxima for these concentrations is expected to

fall below 5°C and the τ_R approaches a very large value (e.g., ~67 s) for a 25 wt% system at 5°C, which indicates the presence of very long micelles.

The observed trend in τ_R clearly suggests that with increasing temperature some structural modifications occur in the network that allow the system to release the stress quickly. The shortening of micelles is not possible because the continuous growth of G_0 clearly indicates that network density increases with temperature. These results are consistent with the formation of micellar joints or branching because sliding of the branching point along the micellar length can provide a fast stress relaxation mechanism.

The variation of microstructural changes in shape and size of the micellar aggregates of 1 wt% surfactant solution at different temperatures (namely, 15, 35, 45, and 55°C) can be obtained by SAXS technique. These temperatures correspond to the different regions of viscosity temperature curves, namely, the viscosity-growth region (see Figure 1.2), the viscosity-maximum region, the viscosity-decline region after the maximum, and near the phase boundary, respectively. The SAXS data are analysed by the generalized indirect Fourier transformation (GIFT) method [47–49]. Figure 1.5a shows the scattering intensity $I(q)$ – q curves at different temperatures. The absence of a peak or maximum in the low- q regime indicates a negligible interparticle interaction. The decay of $I(q)$ at $\sim q^{-1}$ in the low- q region suggests that the aggregates have rod-like local structure at 15, 35 and 45°C. However, at 55°C, a very small but noticeable increase in the slope in the $q < 0.7 \text{ nm}^{-1}$ region was observed that suggests that the aggregate shape is mainly cylindrical but a lamellar-like structure is gradually developing. Lamellar-like aggregates are characterized by $I(q)$ decaying at $\sim q^{-2}$ in the low- q region. The structural change with increasing temperature can be seen from the corresponding pair-distance distribution function (PDDF), $p(r)$, curves shown in Figure 1.5b. The PDDF patterns at 15, 35 and 45°C exhibit a typical feature of the rod-like particles as illustrated by a pronounced peak in the low- r regime and an extended tail in the high- r side. The distance in the low- r region at which $p(r)$ decreases sharply after the maximum gives a cross-sectional diameter of the aggregates,

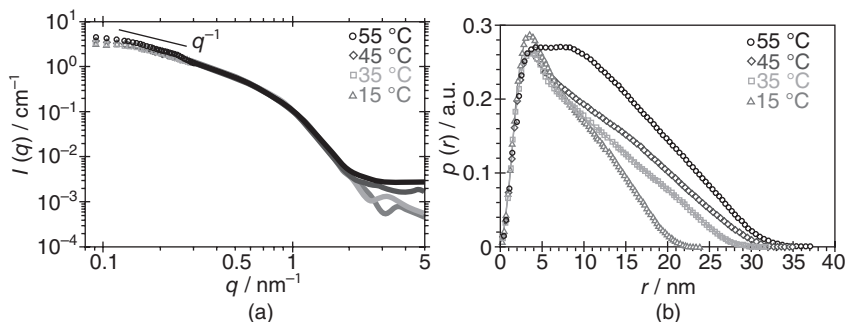


Figure 1.5 (a) Scattered intensity, $I(q)$, from SAXS measurement of the 1wt% surfactant solution at different temperatures and (b) the corresponding pair-distance distribution functions (PDDF), $p(r)$ (from Ref. [37]).

whereas the value of r at which $p(r)$ becomes zero gives the maximum dimension of the aggregate (D_{\max}), that is, the length of the cylindrical micelles. The PDDFs of the aggregates show that the D_{\max} increases with increasing temperature, but the cylindrical cross-sectional diameter of the rod-like aggregates is almost constant (~ 5.8 nm). The D_{\max} depends on the maximum of resolution (or q_{\min}) of the measurement, and it may not provide the actual length of the micelles, which are believed to have their contour lengths in the several hundred nanometers or even micrometer range. Nevertheless, the observed trends in the variation of D_{\max} values can be taken as evidence of micellar growth. With a further increase in temperature to 55°C , the D_{\max} continues to increase and a bulge in the middle- r region of $p(r)$ function appears. Such a change in the $p(r)$ function suggests a gradual evolution of the local structure toward a lamellar pattern [50].

Temperature-induced micellar growth and evolution of low-curvature structures at higher temperature as obtained by SAXS measurements provide a direct evidence of the formation of micellar joints or branching. Addition of lipophilic nonionic surfactant such as trioxyethylene dodecyl ether to the dilute solutions of several ionic as well as hydrophilic nonionic surfactant induces one-dimensional micellar growth and causes the viscosity to sharply increase to a maximum and then decrease [23, 25, 26, 30, 31]. Finally, a two-phase region consisting of aggregates with low curvature (L_α phase or vesicles) and a micellar solution appears. The mechanism of transformation of worm-like micelles to structures with low curvature is still not clearly understood. Most probably, formation of micellar joints and the growth of the joints to a bilayer structure is the mechanism. It is reasonable to expect a similar type of structural evolution in the present system because increasing temperature and the addition of a lipophilic surfactant both decrease the interfacial curvature of the aggregates.

1.4

Viscoelastic Worm-Like Micelles in Mixed Nonionic Fluorinated Surfactant Systems

Mixtures of perfluoroalkyl sulfonamide ethoxylates, $\text{C}_8\text{F}_{17}\text{SO}_2\text{N}(\text{C}_3\text{H}_7)(\text{C}_2\text{H}_4\text{O})_n\text{H}$ (abbreviated as $\text{C}_8\text{F}_{17}\text{EO}_n$, $n = 20, 1$, and 3) are known to form viscoelastic worm-like micelles in water [51, 52]. Incorporation of a cosurfactant in the palisade layer of micellar aggregates reduces the effective area per molecule a_s , which results in a decrease in the interfacial curvature of the aggregate, thus leading to micellar growth. Partial ternary phase diagrams of water/ $\text{C}_8\text{F}_{17}\text{EO}_{20}$ / $\text{C}_8\text{F}_{17}\text{EO}_1$ and water/ $\text{C}_8\text{F}_{17}\text{EO}_{20}$ / $\text{C}_8\text{F}_{17}\text{EO}_3$ systems at 25°C are shown in Figure 1.6.

In water/ $\text{C}_8\text{F}_{17}\text{EO}_{20}$ binary system, a micellar solution (W_m) is formed over a wide range of surfactant concentration at 25°C . Because of the very big headgroup, $\text{C}_8\text{F}_{17}\text{EO}_{20}$ forms globular types of micelles above the critical micelle concentration (CMC), which has been found to be 0.023 mM at 25°C despite its bulky and stiff fluorocarbon chain [53]. The detailed aqueous binary phase behavior and the micellar structure of the $\text{C}_8\text{F}_{17}\text{EO}_{20}$ in water are described elsewhere [54]. The micellar solution of $\text{C}_8\text{F}_{17}\text{EO}_{20}$ can solubilize a significant amount of $\text{C}_8\text{F}_{17}\text{EO}_1$ or

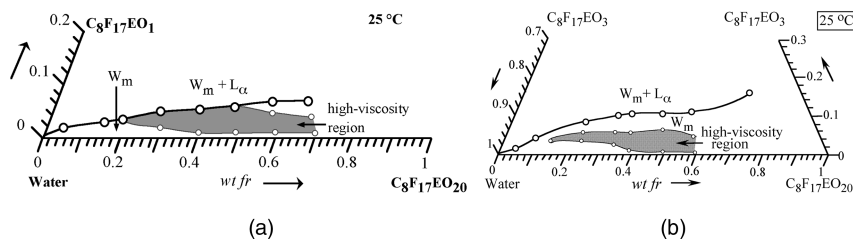


Figure 1.6 Partial phase diagrams of (a) water/ $C_8F_{17}EO_{20}/C_8F_{17}EO_1$ and (b) water/ $C_8F_{17}EO_{20}/C_8F_{17}EO_3$ ternary systems. W_m stands for the isotropic micellar solution and L_α is the lamellar liquid-crystalline phase (redrawn from Ref. [51, 52]).

$C_8F_{17}EO_3$, which is evident from the height of the W_m domain in the ternary phase diagram. Due to the bulky and stiff hydrophobic tail and small hydrophilic group, $C_8F_{17}EO_1$ or $C_8F_{17}EO_3$ itself cannot form discrete aggregates in water. Due to the same reason, incorporation of $C_8F_{17}EO_1$ or $C_8F_{17}EO_3$ in the aggregates of $C_8F_{17}EO_{20}$ reduces the average headgroup area at the interface or, in other words, reduces the interfacial curvature, and beyond the solubilization limit of the W_m phase, the L_α phase separates out from the isotropic solution. Upon successive addition of $C_8F_{17}EO_1$ or $C_8F_{17}EO_3$ to the micellar solution of $C_8F_{17}EO_{20}$, no significant change in viscosity occurs in the dilute solution of the surfactant, but at higher concentration (above 15 or 20 wt% of $C_8F_{17}EO_{20}$), viscosity increases gradually at first, then promptly and a viscous solution is observed. The shaded area in the phase diagrams shows the approximate region of viscous solution inside the W_m domain. The samples inside the high-viscosity zone show flow-birefringence, which is seen when the samples are viewed under crossed polarizers while being shaken. With further addition of $C_8F_{17}EO_1$ or $C_8F_{17}EO_3$ viscosity decreases and ultimately a phase separation occurs. It should be noted that the range of surfactant concentrations in which viscoelastic worm-like micellar solutions are formed is much higher than the range reported in the literature.

Figure 1.7 shows the variation of zero-shear viscosity (η_0) as a function of the weight fraction of $C_8F_{17}EO_1$ in total surfactant, W at two different $C_8F_{17}EO_{20}$ concentrations (25 and 35 wt%). It can be seen that above a certain value of W , the viscosity increases steeply and attains the maximum, followed by a decline. When $C_8F_{17}EO_{20}$ concentration is increased from 25 to 35 wt%, a rapid viscosity growth occurs at lower concentration of $C_8F_{17}EO_1$, or in other words, the η_0 - W curve shifts toward lower W values, which can be attributed to the decrease in the effective cross-sectional area per surfactant molecule (a_s) in the aggregate with increasing concentration of $C_8F_{17}EO_{20}$. The trend is essentially similar to that observed in the worm-like micellar solutions formed in mixed systems of hydrocarbon surfactants. At compositions around the viscosity maxima the systems exhibit viscoelasticity.

Figure 1.8 shows the change in G_0 and τ_R with W for 35 wt% $C_8F_{17}EO_{20} + C_8F_{17}EO_1$ and 25 wt% $C_8F_{17}EO_{20} + C_8F_{17}EO_1$ systems. These parameters were estimated by fitting of the experimental data from frequency-sweep measurements, especially

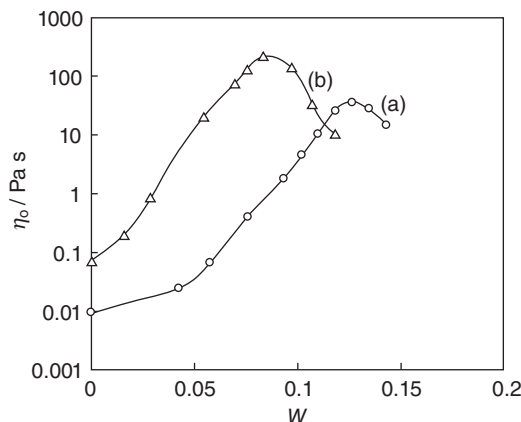


Figure 1.7 Variation of zero-shear viscosity (η_0) as a function of the weight fraction of $C_8F_{17}EO_1$ in total surfactant, W for the (a) 25 wt% $C_8F_{17}EO_{20} + C_8F_{17}EO_1$ and (b) 35 wt% $C_8F_{17}EO_{20} + C_8F_{17}EO_1$ systems at 25 °C (from Ref. [51]).

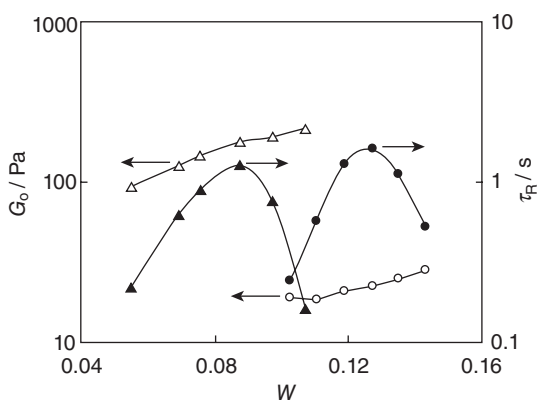


Figure 1.8 Variation of shear modulus (G_0) and relaxation time (τ_R) as a function of the mixing fraction of $C_8F_{17}EO_1$ in total surfactant (W) in the (a) 25 wt% $C_8F_{17}EO_{20} + C_8F_{17}EO_1$ and (b) 35 wt% $C_8F_{17}EO_{20} + C_8F_{17}EO_1$ systems at 25 °C. Solid lines are given for visual guide only (from Ref. [51]).

the data in the low-frequency region, to the Maxwell equations. The shift of the η_0 and τ_R curves toward the lower W values in the η_0 - W (Figure 1.7) and τ_R - W (Figure 1.8) plots upon increasing the $C_8F_{17}EO_{20}$ concentration in the mixed system corresponds to the higher extent of micellar growth. This is also obvious from the increase in G_0 or network density upon increasing surfactant concentration. The lower value of τ_R at the maximum in the 35 wt% $C_8F_{17}EO_{20} + C_8F_{17}EO_1$ system in comparison to that in the 25 wt% $C_8F_{17}EO_{20} + C_8F_{17}EO_1$ system should not be considered as a lower extent of micellar growth in the former system. Instead, it might have arisen from the fact that with increasing surfactant concentration the

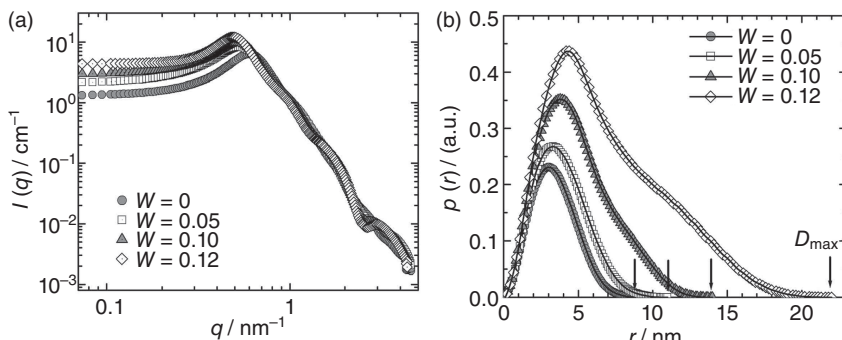


Figure 1.9 (a) Normalized X-ray scattered intensities, $I(q)$ of the 25 wt% $\text{C}_8\text{F}_{17}\text{EO}_{20} + \text{C}_8\text{F}_{17}\text{EO}_1$ system at different weight fraction of $\text{C}_8\text{F}_{17}\text{EO}_1$ in total

surfactant, W at 25 °C and (b) the corresponding PDDF, $p(r)$, functions. The arrows in panel “b” represent the maximum dimension of the micelles (from Ref. [54]).

spontaneous curvature decreases and the system favors the micellar branching at lower values of W in order to minimize the energy cost of the formation of end-caps. Continuous growth of G_0 in the given composition range where η_0 and τ_R decrease shows that after branching the network density grows until the phase separation occurs. There are indications that the local structure at branching points evolve toward bilayer structure [37] and ultimately separates out. The viscosity growth, and the change of G_0 and τ_R as a function of the mixing fraction of $\text{C}_8\text{F}_{17}\text{EO}_3$ in total surfactant (W) for the 25 wt% $\text{C}_8\text{F}_{17}\text{EO}_{20} + \text{C}_8\text{F}_{17}\text{EO}_3$ and the 35 wt% $\text{C}_8\text{F}_{17}\text{EO}_{20} + \text{C}_8\text{F}_{17}\text{EO}_3$ systems at 25 °C show a similar trend to that obtained for the water/ $\text{C}_8\text{F}_{17}\text{EO}_{20}$ / $\text{C}_8\text{F}_{17}\text{EO}_1$ system.

A supportive structural evidence for the rheological data of worm-like micelles can be obtained from SAXS technique for the water/ $\text{C}_8\text{F}_{17}\text{EO}_{20}$ / $\text{C}_8\text{F}_{17}\text{EO}_1$ ternary system [54]. Figure 1.9 shows scattering functions, $I(q)$, and the corresponding pair-distance distribution functions (PDDF), $p(r)$, deduced with the GIFT (generalized indirect Fourier transformation) analysis of the SAXS data for 25 wt% $\text{C}_8\text{F}_{17}\text{EO}_{20} + \text{C}_8\text{F}_{17}\text{EO}_1$ systems at different W at 25 °C.

The local maximum in the scattering functions at $\sim 0.5 \text{ nm}^{-1}$ is a clear signature of strong intermicellar interactions, which is quite unavoidable as the system is concentrated (25 wt% $\text{C}_8\text{F}_{17}\text{EO}_{20}$). On increasing the value of W from $W = 0.05$ to 0.12, the interaction peaks shift towards forward direction (towards low q) and the forward scattering intensity increases. Such behavior in the scattering function can be taken as evidence of micellar growth. The micellar growth induced by the fluorocarbon cosurfactant $\text{C}_8\text{F}_{17}\text{EO}_1$ can be clearly seen in the $p(r)$ curves shown in Figure 1.9b. A symmetrical, nearly bell-shaped $p(r)$ curve of the 25 wt% surfactant corresponds to the globular or ellipsoid prolate type of micellar structure with nearly homogeneous electron density distribution inside the particle. With increasing W , an asymmetry in the shape of the $p(r)$ curve is developed and grows parallel to the W , indicating the micellar growth. With successive increase of W , D_{max} as indicated by arrows increases, and at $W = 0.12$ (the composition at which

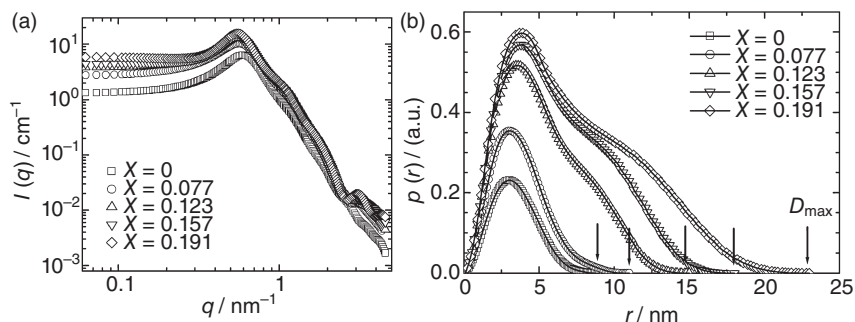


Figure 1.10 (a) Normalized X-ray scattered intensities, $I(q)$ of the 25 wt% $\text{C}_8\text{F}_{17}\text{EO}_{20}$ + $\text{C}_8\text{F}_{17}\text{EO}_3$ system at different weight fraction of $\text{C}_8\text{F}_{17}\text{EO}_3$ in total surfactant, X at 25 °C

and (b) the corresponding PDDF, $p(r)$, functions. The arrows in panel “b” represent the maximum dimension of the micelles (from Ref. [52]).

the maximum viscosity is obtained, see Figure 1.7), D_{max} increases greatly. A pronounced peak in the low- r side with an extended tail in the higher- r side of the $p(r)$ curve is a clear signature of cylindrical micelles. The similar results of scattering functions, $I(q)$, and the corresponding pair-distance distribution functions (PDDF), $p(r)$, of the SAXS data for the 25 wt% $\text{C}_8\text{F}_{17}\text{EO}_{20}$ + $\text{C}_8\text{F}_{17}\text{EO}_3$ systems at different weight fractions of $\text{C}_8\text{F}_{17}\text{EO}_3$ in total surfactants, X at 25 °C are shown in Figure 1.10. Here also, as shown in Figure 1.10a, the forward scattering intensity increases and the interaction peak shifts toward the forward direction (low- q side) with increasing X from $X = 0.077$ to 0.191 indicating micellar growth. As can be seen from Figure 1.10b, when $\text{C}_8\text{F}_{17}\text{EO}_3$ is added, the D_{max} shifts to the higher- r side, and PDDF curves become asymmetric, indicating elongated aggregates.

1.5

Summary

Fluorinated surfactants tend to form aggregates with low curvature, such as cylindrical aggregates, under solution conditions where hydrocarbon surfactants would form spherical aggregates. The packing constraints of the perfluoroalkyl chain is considered to be reason for the formation of flexible cylindrical aggregates in water even at low surfactant concentrations and low temperature for the perfluoroalkyl sulfonamide ethoxylate system, and with an increase surfactant concentrations, these cylindrical micelles undergo one-dimensional growth and form very long and flexible worm-like micelles that entangle and form a network making a viscoelastic solution. The increase in viscosity with increasing temperature for the nonionic surfactant system is mainly attributed to the decrease in the spontaneous curvature of the aggregates and increased energy cost for the formation of hemispherical end-caps and consequently favors one-dimensional growth. Above a certain temperature, viscosity begins to decrease, not because of the shrinking of

micelles but because the system tends to eliminate the free ends by forming micellar joints in the network and such changes in the microstructure result in a decrease in the viscosity and stress relaxation time but the network structure is retained. A viscoelastic solution of worm-like micelles is formed in an aqueous solution of highly hydrophilic nonionic fluorinated surfactant, perfluoroalkyl sulfonamide ethoxylate at relatively high surfactant concentration when a hydrophobic amphiphile (cosurfactant) is added. Addition of cosurfactant reduces the interfacial curvature of the aggregates and induces one-dimensional micellar growth. With successive addition of cosurfactant, the viscosity increases rapidly to form viscoelastic solutions, then decreases after the maximum, and ultimately a phase separation occurs. Increasing surfactant or cosurfactant concentration in the mixed nonionic system increases the extent of micellar growth that is mainly attributed to the decrease in the spontaneous curvature of the aggregates and consequently a progressive increase in the energy cost for the formation of the hemispherical end-caps of the aggregates.

References

- 1 Israelachvili, J.N., Mitchell, D.J., and Ninham, B.W. (1976) *J. Chem. Soc., Faraday Trans. 2*, **72**, 1525.
- 2 Shinoda, K., Hato, M., and Hayashi, T. (1972) *J. Phys. Chem.*, **76**, 909.
- 3 Kunieda, H., and Shinoda, K. (1976) *J. Phys. Chem.*, **80**, 2468.
- 4 Tanford, C. (1980) *The Hydrophobic Effect: Formation of Micelles and Biological Membranes*, 2nd edn, John Wiley & Sons, Inc., New York.
- 5 El Moujahid, C., Ravey, J.C., Schmitt, V., and Stébé, M.J. (1998) *Colloids Surf. A*, **136**, 289.
- 6 Kern, F., Lemarechal, P., Candau, S.J., and Cates, M.E. (1992) *Langmuir*, **8**, 437.
- 7 Khatory, A., Lequeux, F., Kern, F., and Candau, S.J. (1993) *Langmuir*, **9**, 1456.
- 8 Kim, W.-J., Yang, S.-M., and Kim, M. (1997) *J. Colloid Interface Sci.*, **194**, 108.
- 9 Kim, W.-J., and Yang, S.-M. (2000) *J. Colloid Interface Sci.*, **232**, 225.
- 10 Imai, S., and Shikata, T. (2001) *J. Colloid Interface Sci.*, **244**, 399.
- 11 Vethamuthu, M.S., Almgren, M., Brown, W., and Mukhtar, E. (1995) *J. Colloid Interface Sci.*, **174**, 461.
- 12 Hartmann, V., and Cressely, R. (1997) *Colloids Surf. A*, **121**, 151.
- 13 Rehage, H., and Hoffmann, H. (1988) *J. Phys. Chem.*, **92**, 4712.
- 14 Montalvo, G., Rodenas, E., and Valiente, M. (2000) *J. Colloid Interface Sci.*, **227**, 171.
- 15 Ponton, A., Schott, C., and Quemada, D. (1998) *Colloids Surf. A*, **145**, 37.
- 16 Wang, K., Karlsson, G., Almgren, M., and Asakawa, T. (1999) *J. Phys. Chem. B*, **103**, 9237.
- 17 Knoblich, A., Matsumoto, M., Murata, K., and Fujiyoshi, Y. (1995) *Langmuir*, **11**, 2361.
- 18 Hoffmann, H., and Würtz, J. (1997) *J. Mol. Liq.*, **72**, 191.
- 19 Abe, M., Tobita, K., Sakai, H., Kondo, Y., Yoshino, N., Kasahara, Y., Matsuzawa, H., Iwahashi, M., Momozawa, N., and Nishiyama, K. (1997) *Langmuir*, **13**, 2932.
- 20 Tobita, K., Sakai, H., Kondo, Y., Yoshino, N., Iwahashi, M., Momozawa, N., and Abe, M. (1997) *Langmuir*, **13**, 5054.
- 21 Tobita, K., Sakai, H., Kondo, Y., Yoshino, N., Kamogawa, K., Momozawa, N., and Abe, M. (1998) *Langmuir*, **14**, 4753.
- 22 Danino, D., Weihs, D., Zana, R., Orädd, G., Lindblom, G., Abe, M., and Talmon, Y. (2003) *J. Colloid Interface Sci.*, **259**, 382.
- 23 Acharya, D.P., and Kunieda, H. (2003) *J. Phys. Chem. B*, **107**, 10168.
- 24 Acharya, D.P., Hossain, Md.K., Feng, J., Sakai, T., and Kunieda, H. (2004) *Phys. Chem. Chem. Phys.*, **6**, 1627.

- 25 Naito, N., Acharya, D.P., Tanimura, K., and Kunieda, H. (2004) *J. Oleo Sci.*, **53**, 599.
- 26 Maestro, A., Acharya, D.P., Furukawa, H., Gutiérrez, J.M., López-Quintela, M.A., Ishitobi, M., and Kunieda, H. (2004) *J. Phys. Chem. B*, **108**, 14009.
- 27 Herb, C.A., Chen, L.B., and Sun, W.M. (1994) *Structure and Flow in Surfactant Solutions*, C.A. Herb and R.K. Prud'homme (eds), ACS Symposium Series 578, American Chemical Society, Washington, DC, pp. 153–166.
- 28 Rodríguez, C., Acharya, D.P., Hattori, K., Sakai, T., and Kunieda, H. (2003) *Langmuir*, **19**, 8692.
- 29 Acharya, D.P., Hattori, K., Sakai, T., and Kunieda, H. (2003) *Langmuir*, **19**, 9173.
- 30 Acharya, D.P., Sato, T., Kaneko, M., Singh, Y., and Kunieda, H. (2006) *J. Phys. Chem B*, **110**, 754.
- 31 Acharya, D.P., Shiba, Y., Aratani, K., and Kunieda, H. (2004) *J. Phys. Chem. B.*, **108**, 1790.
- 32 Sato, T., Hossain, Md.K., Acharya, D.P., Glatter, O., Chiba, A., and Kunieda, H. (2004) *J. Phys. Chem. B*, **108**, 12927.
- 33 Larson, R.G. (1999) *The Structure and Rheology of Complex Fluids*, Oxford University Press, New York.
- 34 Cates, M.E., and Candau, S.J. (1990) *J. Phys.:Condens. Matter*, **2**, 6869.
- 35 Granek, R., and Cates, M.E. (1992) *J. Chem. Phys.*, **96**, 4758.
- 36 Cates, M.E. (1988) *J. Phys. Fr.*, **49**, 1593.
- 37 Acharya, D.P., Sharma, S.C., Rodríguez -Abreu, C., and Aramaki, K. (2006) *J. Phys. Chem. B*, **110**, 20224.
- 38 Mitchell, D.J., Tiddy, G.J.T., Waring, L., Bostock, T., and MacDonald, M.P. (1983) *J. Chem. Soc., Faraday Trans. 1*, **79**, 975.
- 39 Esquena, J., Rodríguez, C., Solans, C., and Kunieda, H. (2006) *Micropor. Mesopor. Mater.*, **92**, 212.
- 40 Candau, S.J., and Oda, R. (2001) *Colloids Surf. A*, 183–185.
- 41 Khatory, A., Kern, F., Lequeux, F., Appell, J., Porte, G., Morie, N., Otta, A., and Urbach, W. (1993) *Langmuir*, **9**, 933.
- 42 Croce, V., Cosgrove, T., Dreiss, C.A., King, S., Maitland, G., and Hughes, T. (2005) *Langmuir*, **21**, 6762.
- 43 Lin, Z. (1996) *Langmuir*, **12**, 1729.
- 44 Danino, D., Talmon, Y., Levy, H., Beinert, G., and Zana, R. (1995) *Science*, **269**, 1420.
- 45 In, M., Aguerre-Chariol, O., and Zana, R. (1999) *J. Phys. Chem. B*, **103**, 7747.
- 46 Zana, R. (2002) *Adv. Colloid Interface Sci.*, **97**, 205.
- 47 Brunner-Popela, J., and Glatter, O. (1997) *J. Appl. Crystallogr.*, **30**, 431.
- 48 Weyerich, B., Brunner-Popela, J., and Glatter, O. (1999) *J. Appl. Crystallogr.*, **32**, 197.
- 49 Brunner-Popela, J., Mittelbach, R., Strey, R., Schubert, K.-V., Kaler, E.W., and Glatter, O. (1999) *J. Chem. Phys.*, **21**, 10623.
- 50 Moitzi, C., Freiberger, N., and Glatter, O. (2005) *J. Phys. Chem. B*, **109**, 16161.
- 51 Sharma, S.C., Acharya, D.P., and Aramaki, K. (2007) *Langmuir*, **23**, 5324.
- 52 Sharma, S.C., Shrestha, R.G., Shrestha, L.K., and Aramaki, K. (2009) *J. Phys. Chem. B*, **113**, 1615.
- 53 Sharma, S.C., Shrestha, L.K., and Aramaki, K. (2007) *J. Dispersion Sci. Technol.*, **28**, 577.
- 54 Shrestha, R.G., Shrestha, L.K., Sharma, S.C., and Aramaki, K. (2008) *J. Phys. Chem. B*, **112**, 10520.